

Article

Crystal Growth and Associated Properties of a Nonlinear Optical Crystal—Ba₂Zn(BO₃)₂

Weiguo Zhang ¹, Hongwei Yu ¹, Hongping Wu ^{1,2} and P. Shiv Halasyamani ^{1,*}

¹ Department of Chemistry, University of Houston, 112 Fleming Building, Houston, TX 77204-5003, USA; wgzhang82@gmail.com (W.Z.); hwyu15@gmail.com (H.Y.); wuhp@ms.xjb.ac.cn (H.W.)

² Xinjiang Key Laboratory of Electronic Information Materials and Devices, Xinjiang Technical Institute of Physics & Chemistry, Chinese Academy of Sciences, Urumqi 830011, China

* Correspondence: psh@uh.edu; Tel.: +1-713-743-7716

Academic Editors: Helmut Cölfen and Ning Ye

Received: 25 May 2016; Accepted: 10 June 2016; Published: 15 June 2016

Abstract: Crystals of Ba₂Zn(BO₃)₂ were grown by the top-seeded solution growth (TSSG) method. The optimum flux system for growing Ba₂Zn(BO₃)₂ crystals was 2BaF₂:2.5B₂O₃. The transmission spectra of a (100)-orientated crystal indicated an absorption edge of 230 nm. Powder second-harmonic generation measurement revealed that Ba₂Zn(BO₃)₂ can achieve type-I phase matching behavior at the fundamental wavelengths of 1064 and 532 nm respectively. The second-harmonic generating efficiency is around 0.85 and 0.58 times that of β-BaB₂O₄ when radiated with 1064 and 532 nm lasers.

Keywords: crystal growth; top-seeded solution growth method; borates; Ba₂Zn(BO₃)₂; second-harmonic generation

1. Introduction

Nonlinear optical (NLO) materials play a very important role in laser applications owing to their ability to produce coherent light and thus expand the spectral ranges of solid state lasers from ultraviolet (UV) to infrared (IR) [1–4]. Among these NLO materials, borate NLO materials have predominance in UV applications owing to their high UV transmittance and large laser damage threshold (LDT) [2,5]. The first report of NLO phenomena in borates was on KB₅O₈·4H₂O (KB5) [6]. The intense research on the NLO phenomena of borates was triggered by the second-harmonic generation (SHG) reported on β-BaB₂O₄ (β-BBO) and LiB₃O₅ (LBO) in the late 1980s [7,8]. Thereafter, a variety of NLO borate materials have been discovered, such as BaZn₂(BO₃)₂ [9], CsB₃O₅ (CBO) [10], Ba₂Zn(BO₃)₂ [11], KBe₂BO₃F₂ (KBBF) [12], Sr₂Be₂B₂O₇ (SBBO) [13], CsLiB₆O₁₀ (CLBO) [14], K₂Al₂B₂O₇ (KABO) [15], BaAl₂B₂O₇ (BABO) [15], LiAB₄O₇ (A = K, Rb) [16], M₂B₅O₉X (M = Pb, Ca, Sr, Ba; X = Cl, Br) [17], MBi₂B₂O₇ (M = Ca, Sr) [18], Ca₅(BO₃)₃F [19], BiAlGa₂(BO₃)₄ [20], Bi₂ZnOB₂O₆ [21], Ba₃Sr₄(BO₃)₃F₅ [22], BaMBO₃F (M = Zn, Mg) [23], M₃B₆O₁₁F₂ (M = Sr, Ba) [24], K₃B₆O₁₀Cl [25], Li₃Cs₂B₅O₁₀ [26], Li₄Cs₃B₇O₁₄ [27], K₂SrVB₅O₁₂ [28], Pb₄O(BO₃)₂ [29], KSr₄B₃O₉ [30], Ba₄B₁₁O₂₀F [31], Cs₃Zn₆B₉O₂₁ [32], Li₂Sr₄B₁₂O₂₃ [33], Li₄Sr(BO₃)₂ [34] and K₃Ba₃Li₂Al₄B₆O₂₀F [35]. Despite these new borate-based NLO materials, β-BBO, LBO and CLBO are still the most frequently used NLO crystals in UV region, which is attributable to the difficulties of growing high quality crystals or the low transmittance in the UV region. In order to explain the relationship between the microstructure and NLO properties of a crystal, Chen *et al.* proposed an ‘anionic group theory’ which considered the anionic group mainly responsible for the bulk NLO coefficient [36]. According to the anionic group theory, only 10 kinds of (B_xO_y)^{n−} units would be of practical interest to borate NLO materials, *i.e.*, (BO₃)^{3−}, (BO₄)^{5−}, (B₂O₅)^{4−}, (B₂O₇)^{8−}, (B₃O₆)^{3−}, (B₃O₇)^{5−}, (B₃O₈)^{7−}, (B₃O₉)^{9−}, (B₄O₉)^{6−}, and (B₅O₁₀)^{5−} [36]. As some large units can be taken as linked small units, such as (B₃O₉)^{9−} formed by three end-to-end corner-shared BO₄ tetrahedra, microscopic second-order susceptibilities (χ²) and

band gaps (ΔE_g) of four primary borate anionic units were calculated and the relative orders are $\chi^2(\text{B}_3\text{O}_6)^{3-} \approx \chi^2(\text{B}_3\text{O}_7)^{5-} > \chi^2(\text{BO}_3)^{3-} \gg \chi^2(\text{BO}_4)^{5-}$ and $\Delta E_g(\text{BO}_4)^{5-} > \Delta E_g(\text{BO}_3)^{3-} \approx \Delta E_g(\text{B}_3\text{O}_7)^{5-} > \Delta E_g(\text{B}_3\text{O}_6)^{3-}$, respectively [1]. Even though the $(\text{B}_3\text{O}_6)^{3-}$ group has the largest second-order susceptibility, the $(\text{BO}_3)^{3-}$ group seems to be the optimum choice for borate NLO materials based on overall considerations of nonlinearity, birefringence, UV cut-off and laser damage threshold [1,37].

Among the aforementioned newly discovered borates, $\text{Ba}_2\text{Zn}(\text{BO}_3)_2$ crystallizes in the acentric space group, $Pca2_1$, and its structure is composed of ZnO_4 tetrahedra and BO_3 triangles [11]. In addition, thermal analysis indicated that $\text{Ba}_2\text{Zn}(\text{BO}_3)_2$ may congruently melt around 984 °C which provides a piece of crystal grown from melt for structure refinement [11]. Calculated SHG coefficients were also reported, *i.e.*, $d_{24} = 0.61$ pm/V, around one third of d_{11} of β -BBO [11]. Other than the crystal structure, thermal properties and calculated SHG coefficients, neither large size crystals nor other physical properties were reported. Considering that $\text{Ba}_2\text{Zn}(\text{BO}_3)_2$ melts congruently and $(\text{BO}_3)^{3-}$ unit resides in its structure, we suggest that $\text{Ba}_2\text{Zn}(\text{BO}_3)_2$ could be easily grown as large crystals and show a higher SHG efficiency than calculated. In this work, we report on crystal growth as well as physical properties of $\text{Ba}_2\text{Zn}(\text{BO}_3)_2$.

2. Results and Discussion

2.1. Polycrystalline Powder Synthesis and Characterization

Polycrystalline $\text{Ba}_2\text{Zn}(\text{BO}_3)_2$ was synthesized through standard solid-state techniques (see Section 3.1). The powder X-ray diffraction (XRD) pattern of the polycrystalline material is in good agreement with the calculated pattern from the single crystal data (see Figure 1) [11]. As mentioned earlier [11], $\text{Ba}_2\text{Zn}(\text{BO}_3)_2$ melts congruently at 984 °C and $\text{Ba}_2\text{Zn}(\text{BO}_3)_2$ crystals for structure analysis were grown from melt at 1050 °C. 1 g of polycrystalline $\text{Ba}_2\text{Zn}(\text{BO}_3)_2$, placed in a platinum crucible and heated to 1100 °C to determine if a homogenous melt could be obtained. However, a transparent homogenous melt was not obtained even after maintaining the temperature at 1100 °C for 20 h. After slow cooling (50 °C/h) to room temperature, $\text{Ba}_2\text{Zn}(\text{BO}_3)_2$ was partially decomposed even though the main phase did not change according to powder XRD (see Figure 1). The extra peaks indicated by black arrows in the figure are assigned to ZnO (PDF# 79-0206). Therefore, crystals of $\text{Ba}_2\text{Zn}(\text{BO}_3)_2$ cannot simply be grown from its stoichiometric melt.

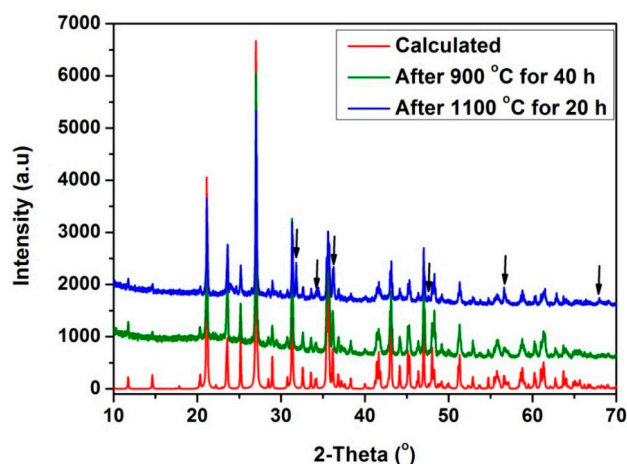


Figure 1. Calculated and experimental XRD of $\text{Ba}_2\text{Zn}(\text{BO}_3)_2$. The black arrows refer to ZnO (PDF# 79-0206).

2.2. Crystal Growth

Our experiments indicate that $\text{Ba}_2\text{Zn}(\text{BO}_3)_2$ does not melt congruently. Therefore, a modified flux method, top-seeded solution growth (TSSG), was employed to grow $\text{Ba}_2\text{Zn}(\text{BO}_3)_2$ crystals.

We attempted many flux systems, such as B_2O_3 , $BaO-B_2O_3$, and $BaF_2-B_2O_3$. When solely taking B_2O_3 as flux, we can obtain $Ba_2Zn(BO_3)_2$ crystals from the system, but the viscosity is very high that prevents growing large and high quality crystals. A $BaO-B_2O_3$ flux also works for growing $Ba_2Zn(BO_3)_2$ crystals. However, adding BaO to the system raised the crystallization temperature and narrowed the growth temperature range. After many attempts, a $BaF_2-B_2O_3$ flux was determined to be optimum to grow $Ba_2Zn(BO_3)_2$ crystals. The proper molar ratio for growing $Ba_2Zn(BO_3)_2$ crystals is $Ba_2Zn(BO_3)_2:B_2O_3:BaF_2 = 15:2.5:2$. Figure 2 shows the as-grown crystals and the powder XRD patterns confirmed its phase (see red pattern in Figure 3). From Figure 2, it is clear that $Ba_2Zn(BO_3)_2$ crystals layer during their growth. The layered face was indexed to be (100) plane (see blue pattern in Figure 3). As discussed earlier [11], the structure of $Ba_2Zn(BO_3)_2$ crystal contains two dimensional layers which are perpendicular to the (100) direction. This may explain the layered growth tendency of $Ba_2Zn(BO_3)_2$ crystals.

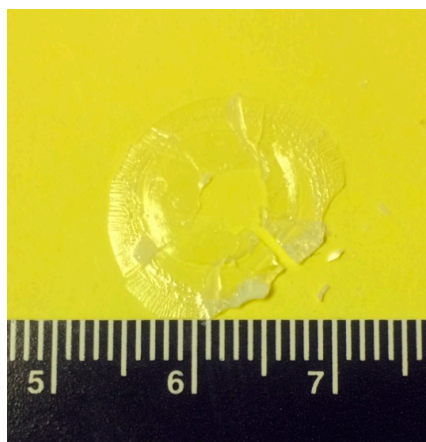


Figure 2. Photo of as-grown $Ba_2Zn(BO_3)_2$ crystals. The minimum scale on the ruler is 1 mm.

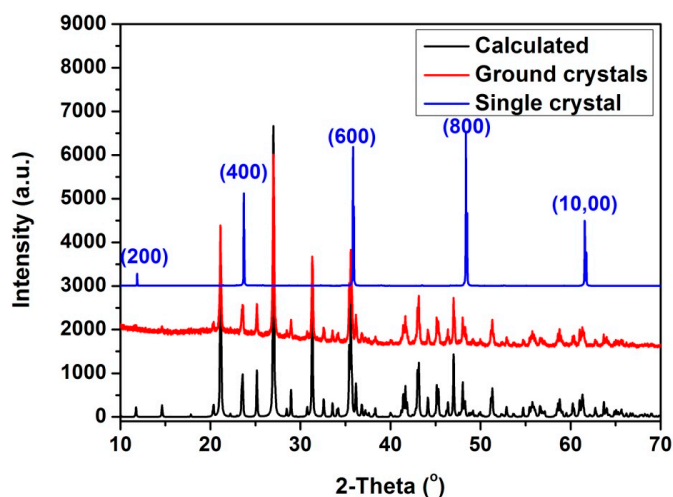


Figure 3. Calculated and experimental XRD patterns of $Ba_2Zn(BO_3)_2$ crystals.

2.3. UV-Visible-Near Infrared Transmission Spectra

The UV-visible-Near infrared (UV-vis-NIR) transmission spectra of an unpolished (100) plate of $Ba_2Zn(BO_3)_2$ with a size of $6 \times 4 \times 0.2 \text{ mm}^3$ indicated that the UV transmission starts to rapidly decrease at around 245 nm and the UV cut-off edge for $Ba_2Zn(BO_3)_2$ is around 230 nm (see Figure 4). According to Chen's calculation, the borates containing $(BO_3)^{3-}$ group could transmit well below 200 nm [1]. This result is consistent with KBBF and KABO crystals where the UV cut-off edges are

155 and 180 nm respectively [38]. However, Chen's calculation did not consider the contribution of transition metals residing in borates to the UV cut-off edge. As the band gap of ZnO is 3.3 eV [39], adding Zn cations to borates may red-shift the UV cut-off edge, e.g., BaZnBO₃F has a UV cut-off edge of 223 nm, whereas BaMgBO₃F has a UV cut-off edge of 190 nm [40,41].

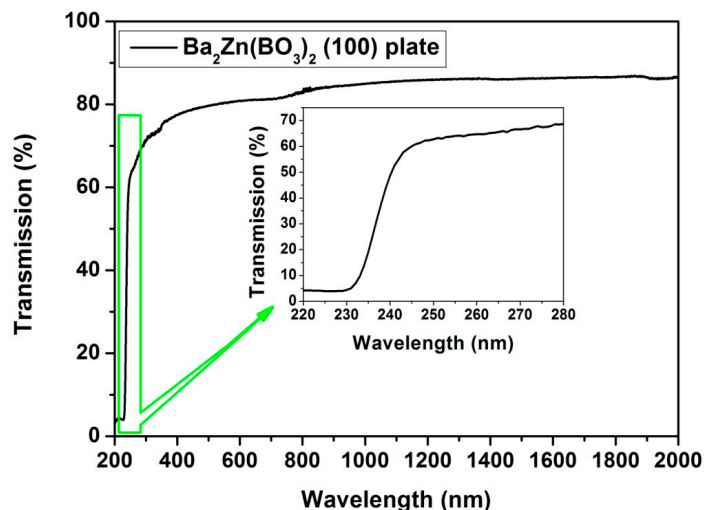


Figure 4. UV-vis-NIR transmission spectra of Ba₂Zn(BO₃)₂ (100) plate. Insert is enlarged UV range.

2.4. Powder SHG Measurements

Powder SHG efficiency *versus* particle size (20–125 μm) (see Figure 5) revealed that Ba₂Zn(BO₃)₂ has an SHG efficiency approximately 0.85 and 1.5 times of β-BaB₂O₄ and KDP when radiated with 1064 nm lasers respectively. While the SHG efficiency of Ba₂Zn(BO₃)₂ is around 0.58 times of β-BaB₂O₄ under the fundamental wavelength of 532 nm. The measurements also indicate Ba₂Zn(BO₃)₂ is type-I phase-matchable at both wavelengths, and falls in the class A category of SHG materials [42]. The decreased SHG efficiency at 532 nm is probably attributable to the slightly decreased transmission at the second harmonic generating wavelength (266 nm) (see Figure 4).

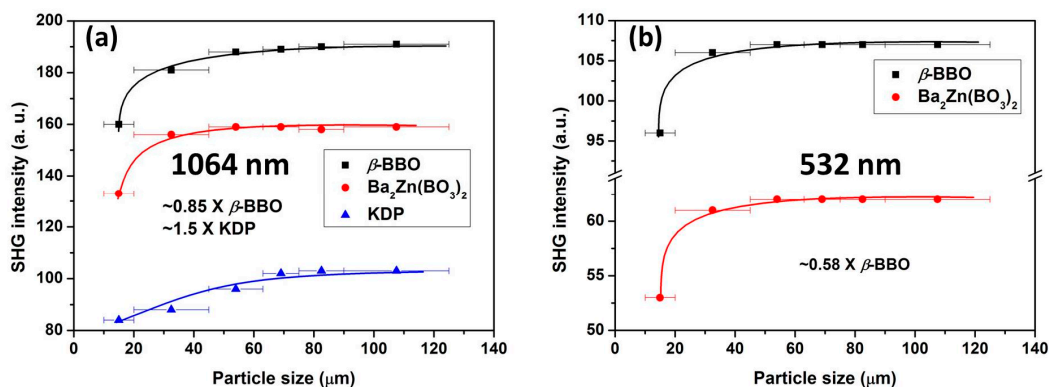


Figure 5. Powder SHG measurement of polycrystalline Ba₂Zn(BO₃)₂ at the fundamental wavelengths of (a) 1064 nm (b) 532 nm. Note the curves are drawn to guide the eye and are not a fit to the data.

3. Materials and Methods

3.1. Materials and Polycrystalline Powder Synthesis

Polycrystalline Ba₂Zn(BO₃)₂ was synthesized by solid-state reaction techniques. Stoichiometric amounts of BaCO₃ (Alfa Aesar, Ward Hill, MA, USA, 99%), ZnO (Alfa Aesar, Ward Hill, MA, USA,

98%) and H_3BO_3 (Alfa Aesar, Ward Hill, MA, USA, 98%) were ground, placed into a platinum crucible, and heated in air to 600 °C for 24 h and 900 °C for 40 h with intermittent re-grindings.

3.2. Powder X-Ray Diffraction

Powder X-ray diffraction measurements were carried out on a PANalytical X'Pert Pro diffractometer (Almelo, The Netherlands) equipped with Cu $K\alpha$ radiation ($\lambda = 1.54056 \text{ \AA}$) in the 2θ range from 10° to 70°.

3.3. Single Crystal Growth of $\text{Ba}_2\text{Zn}(\text{BO}_3)_2$

Polycrystalline $\text{Ba}_2\text{Zn}(\text{BO}_3)_2$, H_3BO_3 , and BaF_2 (Alfa Aesar, 99%) with a molar ratio of 15:5:2 were placed in a platinum crucible, and heated to 950 °C for 24 h in order to form a homogenous melt. Heating BaCO_3 , ZnO , H_3BO_3 and BaF_2 with a molar ratio 30:15:35:2, at a rate of 50 °C/h to 950 °C and holding for 24 h will also form a homogenous melt. Either may be used for the crystal growth. Crystals of $\text{Ba}_2\text{Zn}(\text{BO}_3)_2$ were first grown by spontaneous crystallization, *i.e.*, crystals formed on a platinum wire dipped into the melt. Seed crystals were selected from these spontaneously grown crystals. A crystallization temperature of 937 °C was determined by observing the growth or dissolution of the seed crystals when dipped into the melt. A piece of seed was introduced into the melt at a rotation rate of 10 rpm at 2 °C higher than the crystallization temperature of 937 °C in order to reduce surface defects. The temperature was decreased to the crystallization temperature at a cooling rate of 0.5 °C/min. From the crystallization temperature, the melt was cooled at a rate of 0.5 °C per day to 935 °C. When the crystal growth process was done, *i.e.*, by observing the gap between the growing crystal and the crucible wall (when the crystal edge is very close to the crucible wall the crystal growth is considered complete), the crystal is pulled from the melt and cooled (20 °C/h) to room temperature.

3.4. Optical Spectra Measurement

UV-vis-NIR transmission data were collected on a Varian Cary 5000 scan UV-vis-NIR spectrophotometer (Agilent Technologies, Inc., Santa Clara, CA, USA) over the 200–2000 nm spectral range at room temperature. An unpolished piece of (100) crystal plate with a thickness of 0.2 mm was used to perform the measurement.

3.5. Powder Second Harmonic Generation Measurement

Powder SHG measurements were performed on a modified Kurtz-NLO system [42] using a pulse Nd:YAG laser (Quantel Laser, Ultra 50, Bozeman, MT, USA) with wavelengths of 1064 and 532 nm. A detailed description of the equipment and methodology has been published elsewhere [43]. As the powder SHG efficiency has been shown to depend strongly on particle size, [42] polycrystalline $\text{Ba}_2\text{Zn}(\text{BO}_3)_2$ was ground and sieved into distinct particle size ranges (<20, 20–45, 45–63, 63–75, 75–90, 90–125 μm) to investigate its phase-matching behavior. Polycrystalline β -BBO and KH_2PO_4 (KDP) were also sieved into similar particle sizes for SHG efficiency comparison.

4. Conclusions

$\text{Ba}_2\text{Zn}(\text{BO}_3)_2$ crystals have been grown by the top-seeded solution growth (TSSG) method with $2\text{BaF}_2\text{-}2.5\text{B}_2\text{O}_3$ as flux. The transmission spectra and the powder SHG measurement indicated that $\text{Ba}_2\text{Zn}(\text{BO}_3)_2$ crystal is an attractive candidate for UV NLO optical application. The only issue left to conquer is its layered growth tendency.

Acknowledgments: We thank the Welch Foundation (Grant E-1457), the National Science Foundation (DMR-1503573), and the Texas Center for Superconductivity for support.

Author Contributions: Weiguo Zhang and P. Shiv Halasyamani conceived and designed the experiments; Weiguo Zhang performed the experiments; Hongwei Yu and Hongping Wu contributed reagents/materials/analysis tools; and all authors contributed in the manuscript preparation.

Conflicts of Interest: The authors declare no conflict of interest.

References

1. Chen, C.; Lin, Z.; Wang, Z. The development of new borate-based UV nonlinear optical crystals. *Appl. Phys. B* **2005**, *80*, 1–25. [[CrossRef](#)]
2. Becker, P. Borate Materials in Nonlinear Optics. *Adv. Mater.* **1998**, *10*, 979–992. [[CrossRef](#)]
3. Petrov, V.; Rempel, C.; Stolberg, K.-P.; Schade, W. Widely tunable continuous-wave mid-infrared laser source based on difference-frequency generation in AgGaS₂. *Appl. Opt.* **1998**, *37*, 4925–4928. [[CrossRef](#)] [[PubMed](#)]
4. Gettemy, D.J.; Harker, W.C.; Lindholm, G.; Barnes, N.P. Some Optical Properties of KTP, LiIO₃, and LiNbO₃. *IEEE J. Quantum Electron.* **1988**, *24*, 2231–2237. [[CrossRef](#)]
5. Arun Kumar, R. Borate Crystals for Nonlinear Optical and Laser Applications: A Review. *J. Chem.* **2013**, *2013*, 154862. [[CrossRef](#)]
6. Dewey, C.F.; Cook, W.R.; Hodgson, R.T.; Wynne, J.J. Frequency doubling in KB₅O₈·4H₂O and NH₄B₅O₈·4H₂O to 217.3 nm. *Appl. Phys. Lett.* **1975**, *26*, 714–716. [[CrossRef](#)]
7. Chen, C.; Wu, Y.; Jiang, A.; Wu, B.; You, G.; Li, R.; Lin, S. New nonlinear-optical crystal: LiB₃O₅. *J. Opt. Soc. Am. B* **1989**, *6*, 616–621. [[CrossRef](#)]
8. Chen, C.; Wu, B.; Jiang, A.; You, G. A new-type ultraviolet SHG crystal—β-BaB₂O₄. *Sci. China Ser. B* **1985**, *28*, 235–243.
9. Smith, R.W.; Keszler, D.A. The noncentrosymmetric orthoborate BaZn₂(BO₃)₂. *J. Solid State Chem.* **1992**, *100*, 325–330. [[CrossRef](#)]
10. Wu, Y.; Sasaki, T.; Nakai, S.; Yokotani, A.; Tang, H.; Chen, C. CsB₃O₅: A new nonlinear optical crystal. *Appl. Phys. Lett.* **1993**, *62*, 2614–2615. [[CrossRef](#)]
11. Smith, R.W.; Koliha, L.J. A new noncentrosymmetric orthoborate [Ba₂Zn(BO₃)₂]. *Mater. Res. Bull.* **1994**, *29*, 1203–1210. [[CrossRef](#)]
12. Chen, C.; Wang, Y.; Xia, Y.; Wu, B.; Tang, D.; Wu, K.; Wenrong, Z.; Yu, L.; Mei, L. New development of nonlinear optical crystals for the ultraviolet region with molecular engineering approach. *J. Appl. Phys.* **1995**, *77*, 2268–2272. [[CrossRef](#)]
13. Chen, C.T.; Wang, Y.B.; Wu, B.C.; Wu, K.C.; Zeng, W.L.; Yu, L.H. Design and synthesis of an ultraviolet-transparent nonlinear-optical crystal Sr₂Be₂B₂O₇. *Nature* **1995**, *373*, 322–324. [[CrossRef](#)]
14. Tu, J.-M.; Keszler, D.A. CsLiB₆O₁₀: A noncentrosymmetric polyborate. *Mater. Res. Bull.* **1995**, *30*, 209–215. [[CrossRef](#)]
15. Ye, N.; Zeng, W.; Wu, B.; Chen, C. Two new nonlinear optical crystals: BaAl₂B₂O₇ and K₂Al₂B₂O₇. *SPIE* **1998**, *3556*, 21–23.
16. Ono, Y.; Nakaya, M.; Sugawara, T.; Watanabe, N.; Siraishi, H.; Komatsu, R.; Kajitani, T. Structural study of LiKB₄O₇ and LiRbB₄O₇: New nonlinear optical crystals. *J. Cryst. Growth* **2001**, *229*, 472–476. [[CrossRef](#)]
17. Plachinda, P.A.; Dolgikh, V.A.; Stefanovich, S.Y.; Berdonosov, P.S. Nonlinear-optical susceptibility of hilgardite-like borates M₂B₅O₉X (M = Pb, Ca, Sr, Ba; X = Cl, Br). *Solid State Sci.* **2005**, *7*, 1194–1200. [[CrossRef](#)]
18. Barbier, J.; Cranswick, L.M. D. The non-centrosymmetric borate oxides, MBi₂B₂O₇ (M = Ca, Sr). *J. Solid State Chem.* **2006**, *179*, 3958–3964. [[CrossRef](#)]
19. Chen, G.; Wu, Y.; Fu, P. Growth and characterization of a new nonlinear optical crystal Ca₅(BO₃)₃F. *J. Cryst. Growth* **2006**, *292*, 449–453. [[CrossRef](#)]
20. Wang, S.; Ye, N. Nonlinear optical crystal BiAlGa₂(BO₃)₄. *Solid State Sci.* **2007**, *9*, 713–717. [[CrossRef](#)]
21. Li, F.; Hou, X.; Pan, S.; Wang, X. Growth, Structure, and Optical Properties of a Congruent Melting Oxyborate, Bi₂ZnOB₂O₆. *Chem. Mater.* **2009**, *21*, 2846–2850. [[CrossRef](#)]
22. Zhang, G.; Liu, Z.; Zhang, J.; Fan, F.; Liu, Y.; Fu, P. Crystal Growth, Structure, and Properties of a Non-Centrosymmetric Fluoride Borate, Ba₃Sr₄(BO₃)₃F₅. *Cryst. Growth Des.* **2009**, *9*, 3137–3141. [[CrossRef](#)]
23. Li, R.K.; Chen, P. Cation Coordination Control of Anionic Group Alignment to Maximize SHG Effects in the BaMBO₃F (M = Zn, Mg) Series. *Inorg. Chem.* **2010**, *49*, 1561–1565. [[CrossRef](#)] [[PubMed](#)]

24. McMillen, C.D.; Stritzinger, J.T.; Kolis, J.W. Two Novel Acentric Borate Fluorides: $M_3B_6O_{11}F_2$ ($M = Sr, Ba$). *Inorg. Chem.* **2012**, *51*, 3953–3955. [[CrossRef](#)] [[PubMed](#)]
25. Wu, H.; Pan, S.; Poeppelmeier, K.R.; Li, H.; Jia, D.; Chen, Z.; Fan, X.; Yang, Y.; Rondinelli, J.M.; Luo, H. $K_3B_6O_{10}Cl$: A new structure analogous to perovskite with a large second harmonic generation response and deep UV absorption edge. *J. Am. Chem. Soc.* **2011**, *133*, 7786–7790. [[CrossRef](#)] [[PubMed](#)]
26. Yang, Y.; Pan, S.; Hou, X.; Wang, C.; Poeppelmeier, K.R.; Chen, Z.; Wu, H.; Zhou, Z. A congruently melting and deep UV nonlinear optical material: $Li_3Cs_2B_5O_{10}$. *J. Mater. Chem.* **2011**, *21*, 2890–2894. [[CrossRef](#)]
27. Yang, Y.; Pan, S.; Li, H.; Han, J.; Chen, Z.; Zhao, W.; Zhou, Z. $Li_4Cs_3B_7O_{14}$: Synthesis, crystal structure, and optical properties. *Inorg. Chem.* **2011**, *50*, 2415–2419. [[CrossRef](#)] [[PubMed](#)]
28. Chen, S.; Pan, S.; Zhao, W.; Yu, H.; Wu, H.; Yang, Z.; Yang, Y. A new noncentrosymmetric vanadoborate: Synthesis, crystal structure and characterization of $K_2SrVB_5O_{12}$. *Dalton. Trans.* **2012**, *41*, 9202–9208. [[CrossRef](#)] [[PubMed](#)]
29. Yu, H.; Pan, S.; Wu, H.; Zhao, W.; Zhang, F.; Li, H.; Yang, Z. A new congruent-melting oxyborate, $Pb_4O(BO_3)_2$ with optimally aligned BO_3 triangles adopting layered-type arrangement. *J. Mater. Chem.* **2012**, *22*, 2105–2110. [[CrossRef](#)]
30. Zhao, W.; Pan, S.; Wang, Y.; Yang, Z.; Wang, X.; Han, J. Structure, growth and properties of a novel polar material, $KSr_4B_3O_9$. *J. Solid State Chem.* **2012**, *195*, 73–78. [[CrossRef](#)]
31. Wu, H.; Yu, H.; Yang, Z.; Hou, X.; Su, X.; Pan, S.; Poeppelmeier, K.R.; Rondinelli, J.M. Designing a Deep Ultraviolet Nonlinear Optical Material with Large Second Harmonic Generation Response. *J. Am. Chem. Soc.* **2013**, *135*, 4215–4218. [[CrossRef](#)] [[PubMed](#)]
32. Yu, H.; Wu, H.; Pan, S.; Yang, Z.; Hou, X.; Su, X.; Jing, Q.; Poeppelmeier, K.R.; Rondinelli, J.M. $Cs_3Zn_6B_9O_{21}$: A Chemically Benign Member of the KBBF Family Exhibiting the Largest Second Harmonic Generation Response. *J. Am. Chem. Soc.* **2014**, *136*, 1264–1267. [[CrossRef](#)] [[PubMed](#)]
33. Zhang, M.; Pan, S.; Han, J.; Yang, Z.; Su, X.; Zhao, W. $Li_2Sr_4B_{12}O_{23}$: A new alkali and alkaline-earth metal mixed borate with $[B_{10}O_{18}]^{6-}$ network and isolated $[B_2O_5]^{4-}$ unit. *J. Solid State Chem.* **2012**, *190*, 92–97. [[CrossRef](#)]
34. Zhao, S.; Gong, P.; Bai, L.; Xu, X.; Zhang, S.; Sun, Z.; Lin, Z.; Hong, M.; Chen, C.; Luo, J. Beryllium-free $Li_4Sr(BO_3)_2$ for deep-ultraviolet nonlinear optical applications. *Nat. Comm.* **2014**, *5*, 4019. [[CrossRef](#)] [[PubMed](#)]
35. Zhao, S.; Kang, L.; Shen, Y.; Wang, X.; Asghar, M.A.; Lin, Z.; Xu, Y.; Zeng, S.; Hong, M.; Luo, J. Designing a Beryllium-Free Deep-Ultraviolet Nonlinear Optical Material without a Structural Instability Problem. *J. Am. Chem. Soc.* **2016**, *138*, 2961–2964. [[CrossRef](#)] [[PubMed](#)]
36. Chen, C.; Wu, Y.; Li, R. The anionic group theory of the non-linear optical effect and its applications in the development of new high-quality NLO crystals in the borate series. *Int. Rev. Phys. Chem.* **1989**, *8*, 65–91. [[CrossRef](#)]
37. Xia, Y.; Chen, C.; Tang, D.; Wu, B. New nonlinear optical crystals for UV and VUV harmonic generation. *Adv. Mater.* **1995**, *7*, 79–81. [[CrossRef](#)]
38. Wang, G.L.; Zhang, C.Q.; Chen, C.T.; Xu, Z.Y.; Wang, J.Y. Determination of nonlinear optical coefficients of $KBe_2BO_3F_2$ crystals. *Chin. Phys. Lett.* **2003**, *20*, 243–245.
39. Srikant, V.; Clarke, D.R. On the optical band gap of zinc oxide. *J. Appl. Phys.* **1998**, *83*, 5447–5451. [[CrossRef](#)]
40. Xia, M.; Li, R.K. Growth, structure and optical properties of nonlinear optical crystal $BaZnBO_3F$. *J. Solid State Chem.* **2016**, *233*, 58–61. [[CrossRef](#)]
41. Zhao, J.; Xia, M.; Li, R.K. Flux growth of a potential nonlinear optical crystal $BaMgBO_3F$. *J. Cryst. Growth* **2011**, *318*, 971–973. [[CrossRef](#)]
42. Kurtz, S.K.; Perry, T.T. A Powder Technique for the Evaluation of Nonlinear Optical Materials. *J. Appl. Phys.* **1968**, *39*, 3798–3813. [[CrossRef](#)]
43. Ok, K.M.; Chi, E.O.; Halasyamani, P.S. Bulk characterization methods for non-centrosymmetric materials: Second-harmonic generation, piezoelectricity, pyroelectricity, and ferroelectricity. *Chem. Soc. Rev.* **2006**, *35*, 710–717. [[CrossRef](#)] [[PubMed](#)]

